Supplement of Atmos. Meas. Tech., 10, 3985–4000, 2017
https://doi.org/10.5194/amt-10-3985-2017-supplement

Atmospheric Measurement Techniques
Open Access
EGU

Supplement of

A new method for atmospheric detection of the CH_3O_2 radical

Lavinia Onel et al.

Correspondence to: Lavinia Onel (chmlo@leeds.ac.uk) and Dwayne Heard (d.e.heard@leeds.ac.uk)

S1 Chemical mechanism used to study the dependence of $[CH_3O]/[CH_3O_2]_0$ at the FAGE detection axis on the concentration of NO

The chemical mechanism assumed to be occurring within FAGE after adding NO ~ 25 mm before the CH_3O detection axis to convert CH_3O_2 into CH_3O is described in Table S1 and by Reactions (R3)–(R4) and (R10)–(R11) in the main text.

Table S1. Reactions and rate coefficients at 298 K, k_{298} (Atkinson et al., 2006), used in the numerical simulations described in Sect. 2.2 of the main text using the numerical integration package Kintecus (Ianni, 2002).

Reaction[a]	k_{298} / molecule^{-1} cm^3 s^{-1}
(R3) $CH_3O_2 + NO \rightarrow CH_3O + NO_2$	7.7×10^{-12}
(R4) $CH_3O + O_2 \rightarrow CH_2O + HO_2$	1.9×10^{-15}
(R10) $CH_3O + NO \rightarrow CH_2O + HNO$	2.3×10^{-12}
(R11) $CH_3O + NO + M \rightarrow CH_3ONO + M$	2.2×10^{-12} [b]

[a] The reactions are numbered to correspond to those in the main text

[b] Calculated for p_{FAGE} = 2.65 Torr

S2 FAGE measurement of OH in the calibration flow tube in the absence/presence of CH_4

In order to calibrate FAGE for the sensitivity towards the detection of methyl peroxy radicals, CH_3O_2, OH was generated in a flow tube by water photolysis at 184.9 nm in synthetic air and in the presence of excess methane. The 184.9 nm light was generated by a Hg Pen–Ray lamp. CH_3O_2 was produced by reactions (R1)–R(2) (the reactions are numbered to correspond to those in the main text).

$$OH + CH_4 \rightarrow CH_3 + H_2O \quad \text{(R1)}$$

$$CH_3 + O_2 + M \rightarrow CH_3O_2 + M \quad \text{(R2)}$$

where M = N_2 or O_2.

OH was measured in the absence and in the presence of CH_4 to determine the conversion fraction of OH into CH_3O_2 for the relevant reaction time. The Hg lamp current was varied between 0–20 mA. Figure S1 shows an example of the OH signal with and without CH_4 added to the gas flow. For a typical concentration of CH_4, 5×10^{16} molecule cm^{-3}, 0.96 ± 0.04 of OH was converted into CH_3O_2 for a reaction time of ~ 11 ms in average.

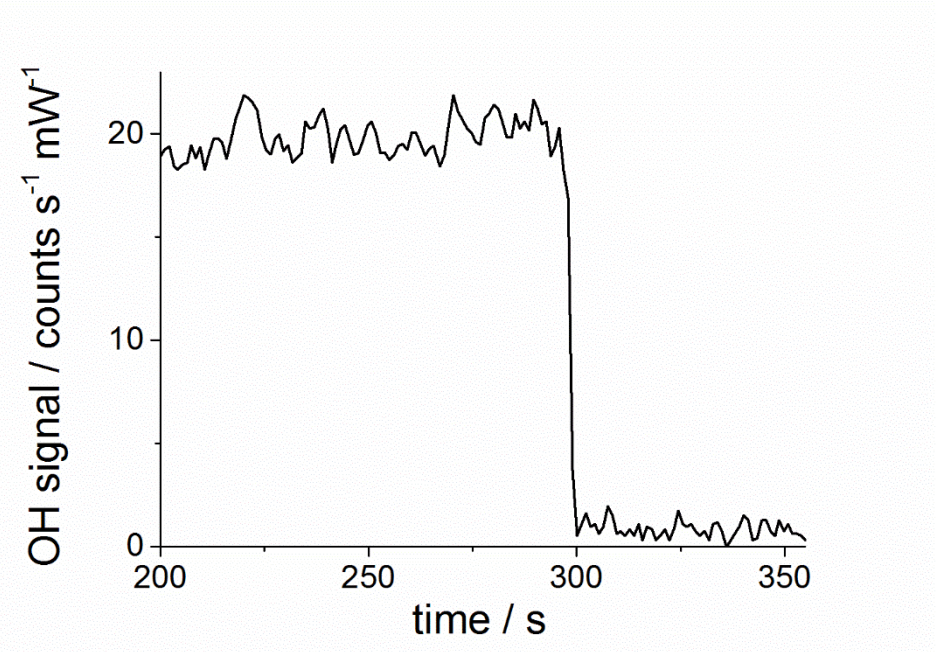

Figure S1. FAGE signal from OH radicals in the absence (until 300 s) and the presence (from 300 s) of 5×10^{16} molecule cm^{-3} CH_4 in the calibration flow tube obtained by flowing 82.5 sccm of CH_4 (main text). The air flow rate in the flow tube was 40 slm giving a reaction time of ~ 11 ms; the concentration of OH in the absence of CH_4 is 4.4×10^8 molecule cm^{-3}, obtained by calibration.

S3 Methyl peroxy calibration using kinetics of the CH_3O_2 second-order decay

The FAGE instrument was coupled to HIRAC to sample the gas with a flow rate of about 3 slm at around 230 mm from the chamber wall. The temporal decays of the CH_3O_2 FAGE signal were generated by turning off the photolysis lamps and analyzed using Eq. (S1) (Eq. (6) in the main paper).

$$\frac{1}{(S_{CH_3O_2})_t} = \frac{1}{(S_{CH_3O_2})_0} + \frac{2 \cdot k_{obs} t}{C_{CH_3O_2}} \qquad \text{or} \qquad (S_{CH_3O_2})_t = 1 \Big/ \left(\frac{1}{(S_{CH_3O_2})_0} + \frac{2 \cdot k_{obs} t}{C_{CH_3O_2}} \right), \tag{S1}$$

In Eq. (S1) $(S_{CH3O2})_t$ and $(S_{CH3O2})_0$ are the signal at time t and $t = 0$, respectively. Eq. (S1) was fitted to the experimental decays (see Fig. S2) of S_{CH3O2}, fixing k_{obs} to the IUPAC recommendation, $k_{obs} = (4.8 \pm 1.1) \times 10^{-13}$ cm^3 $molecule^{-1}$ s^{-1} (Atkinson et al., 2006) and $(S_{CH3O2})_0$ to the mean value of the signal before the lamps were turned off to determine the FAGE sensitivity for CH_3O_2, c_{CH3O2}. Eighteen independent determinations were performed in total with the results presented in Table S2.

Table S2. FAGE sensitivity factors and initial CH_3O_2 concentrations in the HIRAC experiments. Equation (S1) was fitted to the temporal decays of the CH_3O_2 signal to extract C_{CH3O2} and the initial signal, $(S_{CH3O2})_0$, which were then used to determine the initial CH_3O_2 concentrations by using $[CH_3O_2]_0 = (S_{CH3O2})_0/C_{CH3O2}$.

$10^{10} \times C_{CH3O2}$ [a] / counts s^{-1} mW^{-1} cm^3 $molecule^{-1}$	$10^{-11} \times [CH_3O_2]_0$ [b] / molecule cm^{-3}
5.58 ± 0.20	2.63 ± 0.16
4.40 ± 0.47	2.62 ± 0.31
7.04 ± 0.27	2.48 ± 0.16
4.95 ± 0.21	2.40 ± 0.16
6.86 ± 0.18	2.34 ± 0.13
4.54 ± 0.18	2.31 ± 0.15
5.09 ± 0.21	2.19 ± 0.14
5.26 ± 0.21	1.91 ± 0.12
6.11 ± 0.23	1.78 ± 0.11
7.34 ± 0.30	1.71 ± 0.11
7.26 ± 0.25	1.68 ± 0.10
4.92 ± 0.17	1.47 ± 0.09
5.45 ± 0.16	1.41 ± 0.08
5.19 ± 0.16	1.39 ± 0.08
5.42 ± 0.20	1.37 ± 0.06
4.57 ± 0.14	1.34 ± 0.08
5.40 ± 0.23	1.24 ± 0.08
4.83 ± 0.14	1.08 ± 0.06

[a, b] uncertainties quoted to 1σ

S4 Comparison of CH_3O_2 temporal decays for different $[CH_3O_2]_0$

Figure S2 shows the CH_3O_2 FAGE signal decays together with second-order fits recorded for three different $[CH_3O_2]_0$ in HIRAC. The initial signals, $(S_{CH3O2})_0$, were rescaled to start the decays from the same value, $(S'_{CH3O2})_0$ (Eq. (S2)), and show that the temporal decays slow down with the decrease in $[CH_3O_2]_0$ as expected from the dependence of the rate of second–order decays upon $[CH_3O_2]$. Equation (S3) was then fitted to the data shown in Fig. S2 to extract the FAGE sensitivity factor, C_{CH3O2}.

$$(S'_{CH_3O_2})_0 = f \cdot (S_{CH_3O_2})_0 , \quad \text{(S2)}$$

$$(S'_{CH_3O_2})_t = 1 / \left(\frac{1}{(S'_{CH_3O_2})_0} + \frac{2 \cdot k_{obs} t}{f \cdot C_{CH_3O_2}} \right), \quad \text{(S3)}$$

where f is the rescale factor.

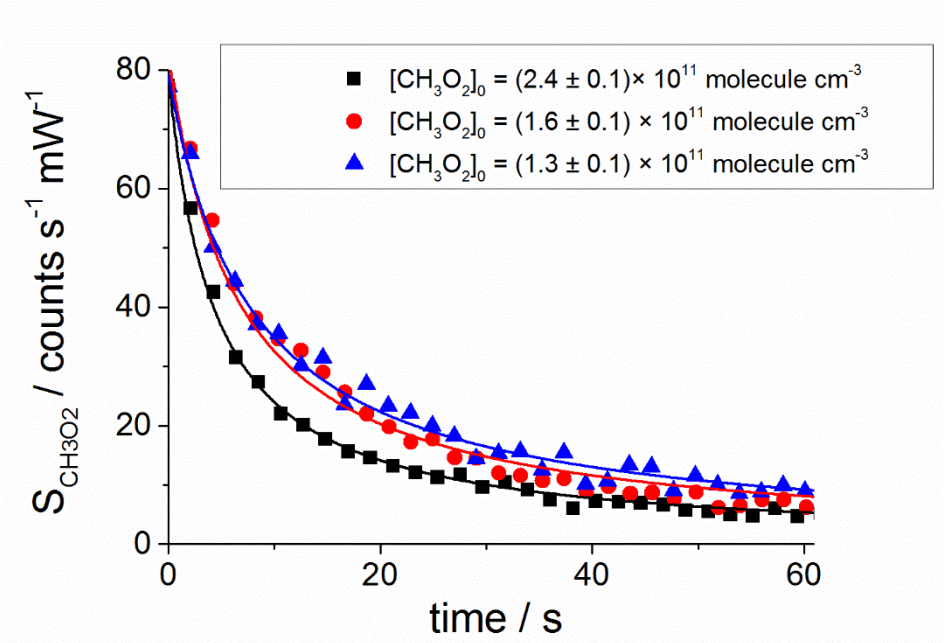

Figure S2. Typical temporal decays of the CH_3O_2 FAGE signal recorded in HIRAC. The experimental data were rescaled to start the decays from the same value, $(S'_{CH_3O_2})_0 = f \cdot (S_{CH_3O_2})_0$, where f is the rescale factor. Equation (S3) was fitted to data to extract the FAGE sensitivity factor, C_{CH3O2} (counts s^{-1} mW^{-1} cm^3 $molecule^{-1}$): $(7.5 \pm 0.1) \times 10^{-10}$ (black line), $(7.3 \pm 0.3) \times 10^{-10}$ (red line) and $(4.5 \pm 0.1) \times 10^{-10}$ (blue line), which was then used to determine the initial CH_3O_2 concentrations presented in the legend by using $[CH_3O_2]_0 = (S_{CH3O2})_0 / C_{CH3O2}$.

S5 Fit of simulated decays of $[CH_3O_2]$ as a function of time

The CH_3O_2 self-reaction occurs through two different channels, (R6.a) and (R6.b) (main text):

$$CH_3O_2 + CH_3O_2 \rightarrow CH_3OH + CH_2O + O_2 \quad \text{(R6.a)}$$

$$CH_3O_2 + CH_3O_2 \rightarrow CH_3O + CH_3O + O_2 \quad \text{(R6.b)}$$

The observed rate coefficient describing the decay of $[CH_3O_2]$ vs. time, k_{obs}, is larger than the second-order rate coefficient of just the CH_3O_2 self-reaction, k_6 and given by Eq. (S4) (Eq. (7) in the main paper) (Sander and Watson, 1981;Lightfoot et al., 1990).

$$k_{obs}=k_6 \cdot (1 + r_{6.b}) \quad \text{(S4)}$$

where $r_{6.b}$ is the branching ratio for the reaction channel R6.b. The IUPAC preferred value is k_{obs} = (4.8 ± 1.1) × 10^{-13} cm^3 $molecule^{-1}$ s^{-1}.

In order to check the validity of Eq. (S4) in the presence of HO_2 removal by self-reaction and wall-loss, numerical simulations were performed to generate CH_3O_2 decays using a system incorporating the chemistry described by Reactions (R4), (R6), R(13) and R(14) shown in the main paper and Table S3 below and a heterogeneous loss of HO_2 ($k_{loss(HO2)}$). The rate coefficients were sourced from the IUPAC recommended values at 298 K (Table S3) and $k_{loss(HO2)}$ was varied. The simulated temporal decays of CH_3O_2 were analysed using Eq. (S5) and gave an average observed rate coefficient of k_{obs} = 4.7 × 10^{-13} cm^3 $molecule^{-1}$ s^{-1}, which is only 2 % lower than the IUPAC recommendation (*vide supra*), for $k_{loss(HO2)}$ in the range 0.01–0.10 s^{-1} and, hence confirmed the applicability of Eq. (S4).

$$[CH_3O_2]_t = 1 / \left(\frac{1}{[CH_3O_2]_0} + \frac{2 \cdot k_{obs} t}{C_{CH_3O_2}}\right), \quad \text{(S5)}$$

A typical simulated decay of CH_3O_2, and the fit to the simulation using Eq. (S5), is shown in Fig. S3.

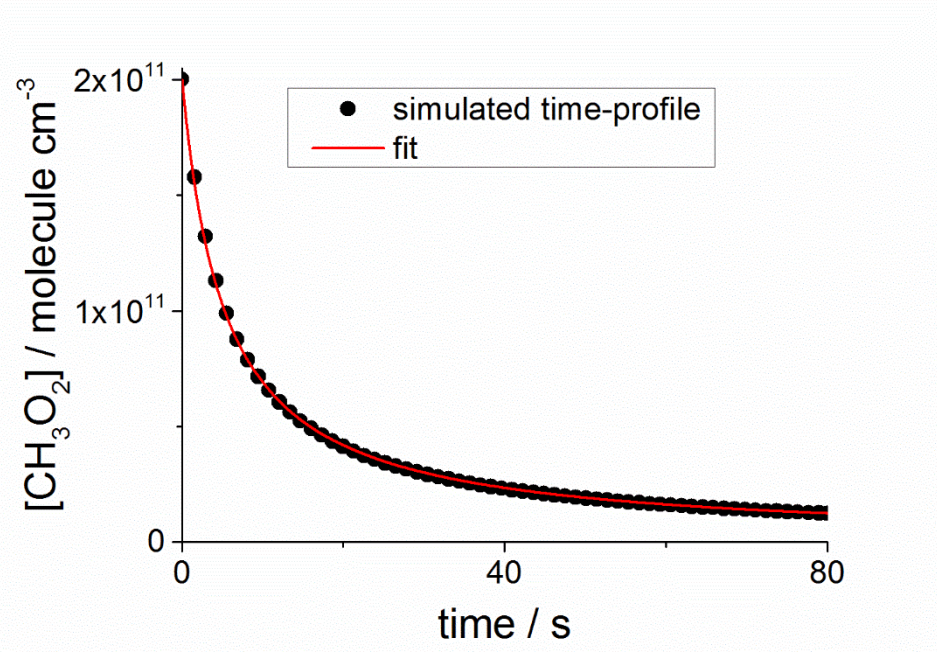

Figure S3. Simulated decay of $[CH_3O_2]$ against time (black circles), using the reactions and the rate coefficients listed in Table S3 and $k_{loss(HO2)}$ = 0.03 s^{-1}, and the fit to the simulation using Eq. (S5) (red line) to determine k_{obs} = 4.7 × 10^{-13} cm^3 $molecule^{-1}$ s^{-1}.

Table S3. Reactions and rate coefficients used in the numerical simulations of the CH_3O_2 temporal decays using the Kintecus package (Ianni, 2002). The rate coefficients are sourced from IUPAC preferred values at 298 K, k_{298}, (Atkinson et al., 2006).

Reaction	k_{298} **/ s^{-1} or molecule^{-1} cm^3 s^{-1}**
(R6.a) $CH_3O_2 + CH_3O_2 \rightarrow CH_2O + CH_3OH + O_2$	2.2×10^{-13}
(R6.b) $CH_3O_2 + CH_3O_2 \rightarrow CH_3O + CH_3O + O_2$	1.3×10^{-13}
(R4) $CH_3O + O_2 \rightarrow CH_2O + HO_2$	1.9×10^{-15}
(R13.a) $CH_3O_2 + HO_2 \rightarrow CH_3OOH + O_2$	4.7×10^{-12}
(R13.b) $CH_3O_2 + HO_2 \rightarrow CH_2O + O_2 + H_2O$	5.2×10^{-13}
(R14.a) $HO_2 + HO_2 \rightarrow H_2O_2 + O_2$	1.6×10^{-12}
(R14.b) $HO_2 + HO_2 + M^a \rightarrow H_2O_2 + O_2 + M$	1.3×10^{-12}

[a] p_{HIRAC} = 1 bar

S6 Chemical mechanism used in numerical simulations to fit the experimental time-profile of the CH_3O concentration shown in Figure 8 of the main paper

In the experiments carried out to measure the concentration of CH_3O generated by the CH_3O_2 self–reaction (Section 3.3 of the main paper) the chamber was filled with high purity N_2. Oxygen was purposely delivered in trace amounts by the incomplete purging of the several meter long pipe delivering N_2. The Cl_2 concentration used in these experiments was 5.6×10^{15} molecule cm^{-3} and hence was 1–2 orders of magnitude higher than $[Cl_2]_0$ used in the CH_3O_2 calibration experiments ($0.3–2.1 \times 10^{14}$ molecule cm^{-3}). Cl atoms were generated by Cl_2 photolysis using black lamps (peak emission wavelength of ~ 360 nm) for the entire experiment to react quickly with CH_4 present in high excess, $[CH_4]_0 = 4.50 \times 10^{17}$ molecule cm^{-3}. Numerical simulations carried out using the chemistry system described in Table S5 (*vide infra*) showed that [Cl] peaked at ~ 2×10^8 molecule cm^{-3} several seconds after starting the experiment (Fig. S5b) followed by a gradual decay.

The experimental temporal profile of CH_3O is shown in Fig. 8 in the main paper and Fig. S4 below. By floating the O_2 concentration until a best–fit was obtained to the experimental data ($r^2 = 0.85$), the numerical simulations determined that the concentration of O_2 in the chamber was $(5.4 \pm 0.6) \times 10^{15}$ molecule cm^{-3}, i.e. around 0.02 % relative to N_2. In the numerical simulations the heterogeneous wall–loss of HO_2 was estimated to be 10^{-2} s^{-1} (Winiberg et al., 2015), with the same value assumed for CH_3O, and the heterogeneous loss of CH_3O_2 was estimated to be 10^{-3} s^{-1} (see main text). The returned best–fit $[O_2]$ did not change by increasing the wall–losses of HO_2, CH_3O and CH_3O_2 by one order of magnitude. Including a heterogeneous removal of Cl atom in the range of (0.001–1) s^{-1} in the model did not change the result of the numerical simulations as the Cl wall–loss could not compete with the Cl + CH_4 reaction; the pseudo–first–order rate coefficient k'_{CH4+Cl} was ~ 4.5×10^4 s^{-1} during the experiment. The wall–

losses of the other species were considered negligible during the 2 min time of the experiment in accordance with previous measurements (Winiberg et al., 2016).

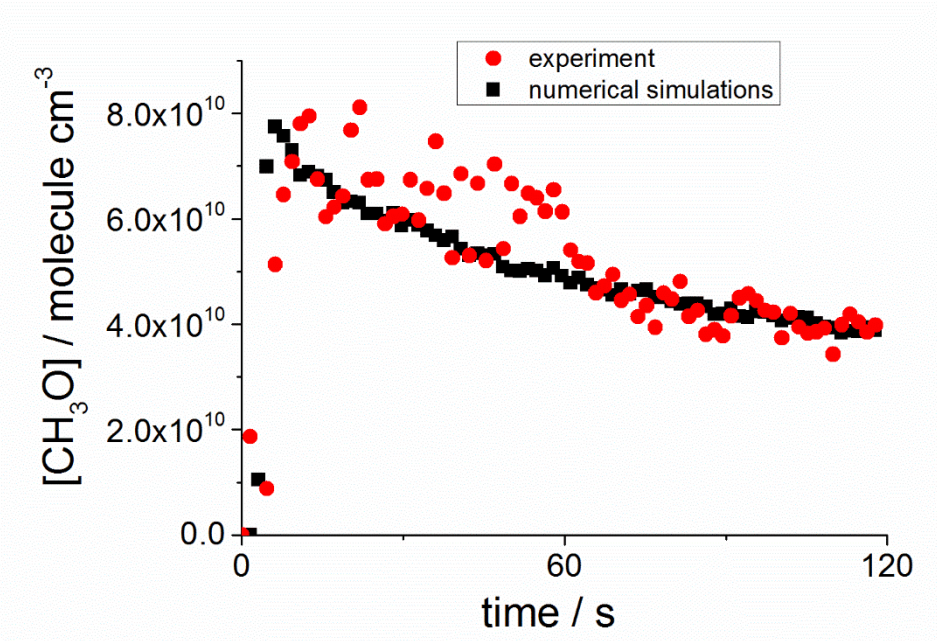

Figure S4. Concentration of CH_3O as a function of time in HIRAC: red points are the experimental data and black points are generated by a numerical simulation. CH_3O radicals were formed as a product of the self-reaction of CH_3O_2 species at 295 K and 1000 mbar of N_2, with CH_3O_2 generated by the reaction of Cl atoms with CH_4, with the HIRAC black lamps being turned on at time zero. Oxygen was present in trace amounts, determined to be $(5.4 \pm 0.6) \times 10^{15}$ molecule cm^{-3} from the simulations fit to the experimental data.

The numerical simulations took into account the increase in intensity of the lamps output during the experiment (Winiberg et al., 2016). In order to numerically simulate the Cl concentration the photolysis rate of Cl_2, $j(Cl_2)$, has been determined by performing separate experiments using the black lamps to simultaneously monitor the decay of CH_2O and the rise of CO during the Cl + CH_2O reaction by using *in situ* FTIR absorption spectroscopy (Glowacki et al., 2007). Numerical simulations have been performed using the reaction rate coefficients from IUPAC (Atkinson et al., 2006) (Table S4) to determine that $j(Cl_2) = (3.8 \pm 1.1) \times 10^{-4}$ s^{-1}. The result is to the same as the value found previously (Winiberg et al., 2016), $(3.8 \pm 1.4) \times 10^{-4}$ s^{-1}, during HIRAC experiments to study the HO_2 + $CH_3C(O)O_2$ reaction.

For the numerically simulated concentration of CH_3, of about 6×10^8 molecule cm^{-3} (Fig. S5c) and the reported rate coefficient for the Cl_2 + CH_3 reaction, $k_{CH3 + Cl2} = 1.5 \times 10^{-12}$ molecule^{-1} cm^3 s^{-1}, (Eskola et al., 2008) the removal of Cl_2 was dominated by the reaction with CH_3. The Cl_2 + CH_3 reaction recycled a Cl atom, which in turn reacted with CH_4 to regenerate more CH_3 radicals leading to the propagation of the Cl – CH_3 chain reaction and increasing the consumption rate of Cl_2. The removal of

Cl_2 by the chain reaction resulted in a relatively sharp decrease of the peak [CH_3O], of about 50 % in 2 min (Fig. S4).

Table S4. Reactions and rate coefficients used in the numerical simulations of the time evolution of the concentrations of CH_2O and CO generated in the $CH_2O/Cl_2/N_2/O_2$ system in HIRAC using the numerical integration package Kintecus to determine $j(Cl_2)$ (Ianni, 2002). The rate coefficients are sourced from the IUPAC preferred values at 298 K, k_{298}, (Atkinson et al., 2006).

Reaction	k_{298} **/ s^{-1} or molecule^{-1} cm^3 s^{-1}**	
$Cl_2 + h\nu \rightarrow 2Cl$	$3.8 \times 10^{-4} = j(Cl_2)$	*a*
$CH_2O + Cl \rightarrow CHO + HCl$	7.2×10^{-11}	
$CHO + O_2 \rightarrow HO_2 + CO$	5.1×10^{-12}	
$HO_2 + HO_2 \rightarrow H_2O_2 + O_2$	1.6×10^{-12}	
$HO_2 + HO_2 + M \rightarrow H_2O_2 + O_2 + M$	1.3×10^{-12}	*b*

[a] $j(Cl_2)$ determined by fitting the [CH_2O] and [CO] vs. time profiles obtained by FTIR measurements within HIRAC; the determined value is equal to the value found previously (Winiberg et al., 2016)
[b] p_{HIRAC} = 1 bar

Table S5. Reactions and rate coefficients used in the numerical simulations of the time evolution of the concentration of CH_3O generated in the $CH_4/Cl_2/N_2/O_2$ system using the Kintecus package (Ianni, 2002). The rate coefficients are sourced from IUPAC preferred values at 298 K, k_{298}, (Atkinson et al., 2006).

Reaction	k_{298} **/ s^{-1} or molecule^{-1} cm^3 s^{-1}**	
$Cl_2 + h\nu \rightarrow 2Cl$	$3.8 \times 10^{-4} = j(Cl_2)$	
$CH_4 + Cl \rightarrow CH_3 + HCl$	1.0×10^{-13}	
$CH_3 + Cl_2 \rightarrow CH_3Cl + Cl$	1.5×10^{-12}	*a*
$CH_3 + O_2 + M \rightarrow CH_3O_2 + M$	7.8×10^{-13}	*b*
$CH_3O_2 + CH_3O_2 \rightarrow CH_2O + CH_3OH + O_2$	2.2×10^{-13}	
$CH_3O_2 + CH_3O_2 \rightarrow CH_3O + CH_3O + O_2$	1.3×10^{-13}	
$CH_3O + O_2 \rightarrow CH_2O + HO_2$	1.9×10^{-15}	
$CH_3O_2 + HO_2 \rightarrow CH_3OOH + O_2$	4.7×10^{-12}	
$CH_3O_2 + HO_2 \rightarrow CH_2O + O_2 + H_2O$	5.2×10^{-13}	
$HO_2 + HO_2 \rightarrow H_2O_2 + O_2$	1.6×10^{-12}	
$HO_2 + HO_2 + M \rightarrow H_2O_2 + O_2 + M$	1.3×10^{-12}	*b*
$CH_2O + Cl + O_2 \rightarrow CO + HO_2 + HCl$	7.2×10^{-11}	*c*
$CH_3OH + Cl + O_2 \rightarrow CH_2O + HO_2 + HCl$	5.5×10^{-11}	*d*
$CH_3OOH + Cl \rightarrow$ Products	5.9×10^{-11}	*e*

[a] (Eskola et al., 2008)

[b] p_{HIRAC} = 1 bar
[c] CH_2O + Cl reaction followed by the HCO + O_2 reaction; the rate–determining step is the CH_2O + Cl reaction
[d] CH_3OH + Cl reaction followed by the CH_2OH + O_2 reaction; the rate–determining step is the CH_3OH + Cl reaction
[e] The dominant channel is assumed to lead to CH_2OOH + HCl (Atkinson et al., 2006). Further decomposition of CH_2OOH may generate OH; the potential secondary chemistry is negligible as [OH] is lower than [Cl] and the rate coefficients of the OH reactions are significantly lower than those of the Cl reactions.

Figure S5 shows the simulated time evolution of Cl_2, Cl, CH_3 and CH_3O_2 over 120 s from these simulations.

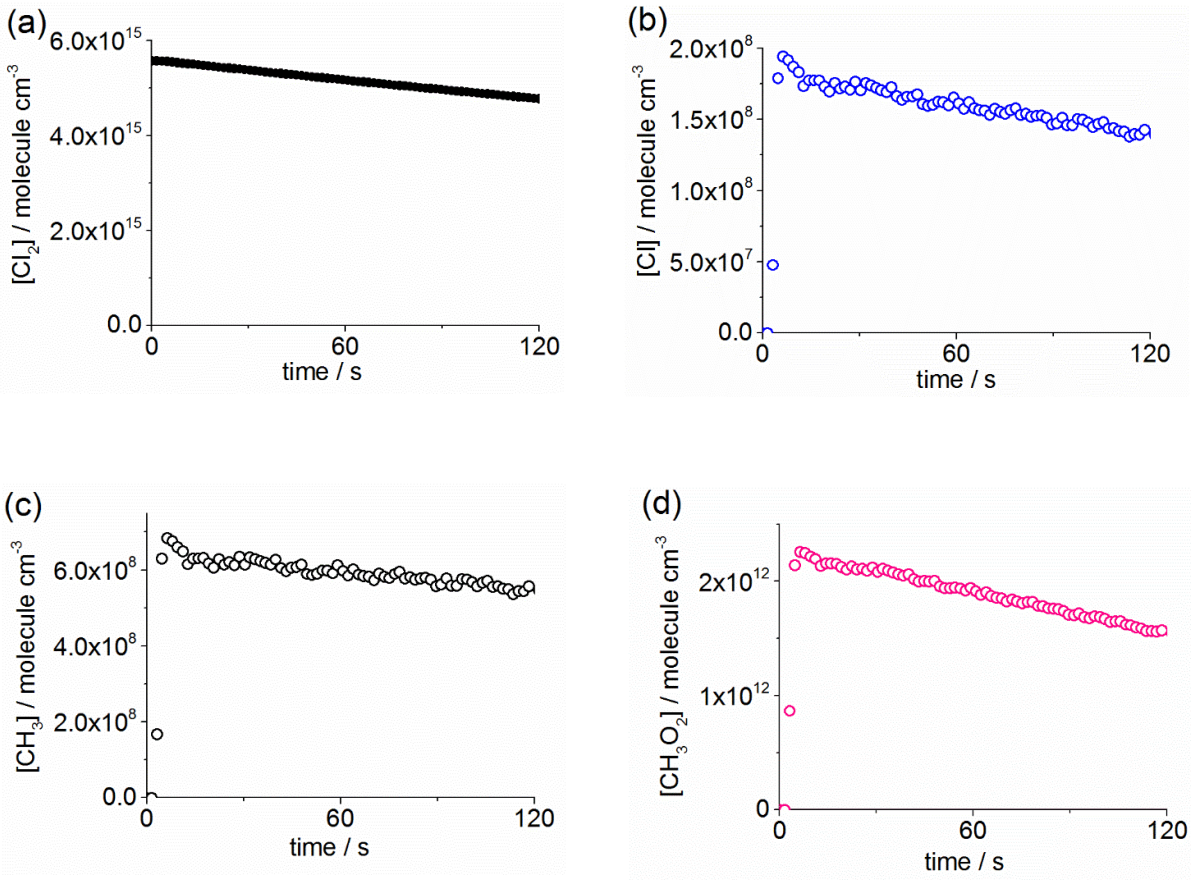

Figure S5. Concentration of (a)Cl_2, (b) Cl, (c) CH_3 and (d) CH_3O_2 as a function of time in HIRAC obtained by numerical simulations using the chemical mechanism and the rate coefficients given in Table S5; $[O_2]_0 = (5.4 \pm 0.6) \times 10^{15}$ molecule cm^{-3}, as obtained by the best–fit to the experimental CH_3O concentrations (Fig. S4).

References

Atkinson, R., Baulch, D. L., Cox, R. A., Crowley, J. N., Hampson, R. F., Hynes, R. G., Jenkin, M. E., Rossi, M. J., and Troe, J.: Evaluated kinetic and photochemical data for atmospheric chemistry: Volume II - gas phase reactions of organic species, Atmos. Chem. Phys., 6, 3625-4055, 2006.

Eskola, A. J., Timonen, R. S., Marshall, P., Chesnokov, E. N., and Krasnoperov, L. N.: Rate constants and hydrogen isotope substitution effects in the CH_3+HCl and CH_3+Cl_2 reactions, J. Phys. Chem. A, 112, 7391-7401, 10.1021/jp801999w, 2008.

Glowacki, D. R., Goddard, A., Hemavibool, K., Malkin, T. L., Commane, R., Anderson, F., Bloss, W. J., Heard, D. E., Ingham, T., Pilling, M. J., and Seakins, P. W.: Design of and initial results from a Highly Instrumented Reactor for Atmospheric Chemistry (HIRAC), Atmospheric Chemistry and Physics, 7, 5371-5390, 2007.

Kintecus, Windows Version 2.80: www.kintecus.com, access: 26/10/2016, 2002.

Lightfoot, P. D., Lesclaux, R., and Veyret, B.: Flash photolysis study of the CH_3O_2 + CH_3O_2 reaction: Rate constants and branching ratios from 248 to 573 K, J. Phys. Chem., 94, 700-707, 10.1021/j100365a035, 1990.

Sander, S. P., and Watson, R. T.: Temperature dependence of the self-reaction of CH_3O_2 radicals, J. Phys. Chem., 85, 2960-2964, 10.1021/j150620a023, 1981.

Winiberg, F. A. F., Smith, S. C., Bejan, I., Brumby, C. A., Ingham, T., Malkin, T. L., Orr, S. C., Heard, D. E., and Seakins, P. W.: Pressure-dependent calibration of the OH and HO_2 channels of a FAGE HOx instrument using the Highly Instrumented Reactor for Atmospheric Chemistry (HIRAC), Atmos. Meas. Tech., 8, 523-540, 10.5194/amt-8-523-2015, 2015.

Winiberg, F. A. F., Dillon, T. J., Orr, S. C., Gross, C. B. M., Bejan, I., Brumby, C. A., Evans, M. J., Smith, S. C., Heard, D. E., and Seakins, P. W.: Direct measurements of OH and other product yields from the HO_2 + $CH_3C(O)O_2$ reaction, Atmos. Chem. Phys., 16, 4023-4042, 2016.